Integrated non-invasive remote-sensing techniques and field survey for the geoarchaeological study of the Sud Lípez mining district, Bolivia



2012 J. Geophys. Eng. 9 S40

(http://iopscience.iop.org/1742-2140/9/4/S40)

IOP Publishing Journal of Geophysics and Engineering
J. Geophys. Eng. **9** (2012) S40–S52 doi:10.1088/1742-2132/9/4/S40

# Integrated non-invasive remote-sensing techniques and field survey for the geoarchaeological study of the Sud Lípez mining district, Bolivia

**Jean-Paul Deroin**[1], **Florian Téreygeol**[2], **Pablo Cruz**[3], **Ivan Guillot**[4] **and Jean-Charles Méaudre**[2]

[1] Université de Reims-Champagne Ardenne, Earth Science Department, EA 3795 GEGENAA, 2 esplanade Roland Garros 51100 Reims, France
[2] UMR 5060 CNRS IRAMAT and CEA, Saclay, France
[3] CONICET INAPL, Buenos Aeres, Argentina
[4] UMR 7182 CNRS ICMPE, Université Paris-Est Créteil, France

E-mail: jean-paul.deroin@univ-reims.fr

Received 7 February 2012
Accepted for publication 8 June 2012
Published 9 August 2012
Online at stacks.iop.org/JGE/9/S40

**Abstract**
New investigations have been carried out in the framework of a joint French–Argentine project dealing with the mineral resources and the metal production in the Andean plateau from the 10th to the 18th century. Geoarchaeology of the Sud Lípez, southern Bolivia, is revisited using multisource remote-sensing data including archive data from the 1960s and recent very high resolution (VHR) data simultaneously acquired with field work. The detailed geological mapping of the area is allowed by the field survey complemented by the multispectral and VHR data. The emphasis is on integrating all the geological features such as morphologies, petrology of the volcanics, lithology of the volcano-sedimentary rocks, regional and local faulting, veins, hydrothermally altered rocks, etc. GeoEye-1, which features the most advanced technology ever used in a civilian remote-sensing system, allows the detailed mapping of the archaeological remains that are particularly numerous at San Antonio de Lípez, with shallow pits, shafts connected in depth with adits, and large slag areas. Particularly, the plan of three old miners' villages has been drawn and its accuracy has been evaluated.

**Keywords:** remote-sensing archaeology, mapping, Corona, Landsat TM, ALOS-AVNIR-2, GeoEye-1, Bolivia, Sud Lípez, San Antonio de Lípez

(Some figures may appear in colour only in the online journal)

## 1. Introduction

Remote-sensing techniques are particularly well adapted for the investigation of remote areas, either for preparing field work or for supporting thematic mapping in the field. Whereas remote sensing is now frequently used in geoarchaeology (Rowlands and Sarris 2007, Lasaponara *et al* 2010, Lasaponara and Masini 2011, 2012, Masini and Soldovieri 2011), relatively few studies have dealt with satellite imagery applied to ancient mining sites. Landsat imagery was used for studying ancient gold mining in Egypt (El Shazly *et al* 1988). As early as the end of the last century, archaeologists began using the new generation of very high resolution (VHR) satellite imagery (Garrison *et al* 2008). Multispectral Landsat data and VHR data from QuickBird have been jointly studied in order to analyse the geological context of the Jabali Zn–Pb–Ag mineralization in Yemen (Deroin *et al* 2011) and the archaeological setting of the site as well (Deroin *et al* 2012).

  

New investigations have been carried out in Bolivia in the framework of a joint French–Argentine project dealing with the mineral resources and the metal production in the Andean plateau. Investigations on the use of geological resources in Latin America are right now focused on the Pre-Spanish period. Previous works in Potosí and Porco have shown the great archaeological potential of these two areas from the 10th to the 18th century. One key result was to emphasize the interest of a comparative study of both the Inca and European technical cultures and the interpenetration of these cultures from the Spanish conquest of the Inca Empire (Van Buren and Mill 2005, Petersen 2010). Our joint French–Argentine project focuses precisely on the technical innovations, continuities and breaks, and their social impact.

In this paper, we investigate ancient sites formerly mined for silver located in the southernmost part of Bolivia. Large-scale remote-sensing surveys have already been conducted on this area using Landsat Thematic Mapper images (Ramos Collorana *et al* 2002). Cáceres *et al* (2004) carried out a more accurate analysis of the San Pablo de Lípez area, which is the main focus of the current mineral exploration (Buena Vista exploration area). They combined the multispectral Landsat data with the hyperspectral data acquired by Aster and found diagnostic spectral signatures of iron oxides (Landsat) and clays and micas (Aster) in relation with the main mineralization.

Our study is based on the use of multisource and multiscale remote-sensing data in order to analyse both local and regional geological settings. The mining sites and their recent evolution (since the 1960s) are surveyed using declassified Corona images and a set of multispectral data in order to detect major exploration phases. Two field missions carried out in 2009 and 2011 were necessary to establish a ground truth for both the geological purpose and the archaeological purpose. The programming of the GeoEye-1 satellite allowed us to acquire a VHR scene on the main test site located in the San Antonio de Lípez–Cerro Lípez area. Three abandoned villages located in the area have been precisely mapped.

## 2. The case study: the Sud Lípez mining district and its silver mines

### *2.1. Location*

The Sud Lípez region of southern Bolivia, near the border with Argentina, corresponds to one of the 16 provinces of the Potosí Department located about 600 km to the south of La Paz (figure 1). This is a remote area in the heart of the central Andes with a very few inhabitants and a density of only 0.3 $km^{-2}$. In that place, the Altiplano joins both the western (*Cordillera Occidental*) and eastern Cordillera (*Cordillera Oriental* also named *Cordillera Real*). This area is sometimes referred to as the central Andean Altiplano–Puna plateau.

From an ecological point of view, the area corresponds to the transition from the Puna region to the high Andean region (Altoandina). The term Puna encompasses diverse ecosystems of the central Andes above 3400 m from northern Peru to northern Argentina and thus crossing southwest Bolivia. The limit with the high Andean region is at about 4200 m. It is noteworthy to point out that the San Antonio de Lípez modern village is precisely located at 4200 m, whereas the main ancient mining sites are located in high mountains with an elevation of at least 4600 m (figure 2). The Puna is dominated by grasses and covers open grassland, cushion vegetation and evergreen resinous shrublands. The Puna is locally grazed by sheep, alpaca and llamas. It includes salt soils and salt flats in the endorheic basins with halophytes and ciénagas and bofedales in the drier part. Above the Puna region grows the sparse vegetation dominated by a few grasses of the high Andean region. Here cushions become dominant. Being more remote, and generally above the limits of human habitation, the high Andean region suffers from only sparse grazing impacts.

### *2.2. Geological setting*

From the Upper Oligocene onward, the collision and subduction of the Nazca plate caused a constant deformation that formed the great volcanic arc along South America's Pacific shoreline. At the heart of this arc, in the so-called Central Volcanic Zone, is the polymetallic belt of the Altiplano and western Cordillera provinces (Ahlfeld 1967). The most important metallogenic features include mineralization of intermediate- and high-sulfidation-type associated with small, shallow subvolcanic plugs, ignimbrite shields, flow domes, stratovolcanoes, and pyroclastic rocks of dacitic, rhyolitic, and andesitic composition (Kussmaul *et al* 1977, Francis and Baker 1978, Baker 1981, Francis *et al* 1983, Hérail *et al* 1996, Riller *et al* 2001, Matteini *et al* 2002, de Silva and Gosnold 2007, Schnurr *et al* 2007, Kay *et al* 2010).

The 800 km × 200 km belt is composed of polymetallic and epithermal vein-type Ag–(Au)–Pb–Zn–Cu deposits. These deposits formed during the Middle–Late Miocene and Early Pliocene, when volcanism led to the formation of widespread precious and base-metal-bearing epithermal deposits (Suarez Soruco 2000, Zappettini 2005). The Sud Lípez mining district is the southernmost mining district of Bolivia (figure 1). It is also the least studied portion of the Altiplano–Puna plateau and contains a number of polymetallic vein-style Ag–Zn–Pb deposits which were exploited for silver (*soroche*) as early as the Inca period, notably at San Antonio de Lípez and San Pablo de Lípez, currently known as Buena Vista (figure 1, nos 1 and 2). Another interesting place is located further east at Santa Isabel where Ag–Au–Sn–Zn mineralization was exploited (figure 1, no 3). Close to the *Salar de Uyuni*, the giant San Cristobal disseminated Ag- and Zn-rich deposit may reflect porphyry dome emplacement into a lacustrine environment (Phillipson and Romberger 2004) (figure 1, no 4). Most deposits exhibit structural control along lineaments, large transcurrent faults such as the Lípez lineament and local-scale tension fractures. Mineralization style varies from vein lodes and stockworks to disseminations in breccias, porous pyroclastics and porphyries.

The Lípez region was the place of a major Neogene ignimbrite flare-up (Salisbury *et al* 2011). Immediately to

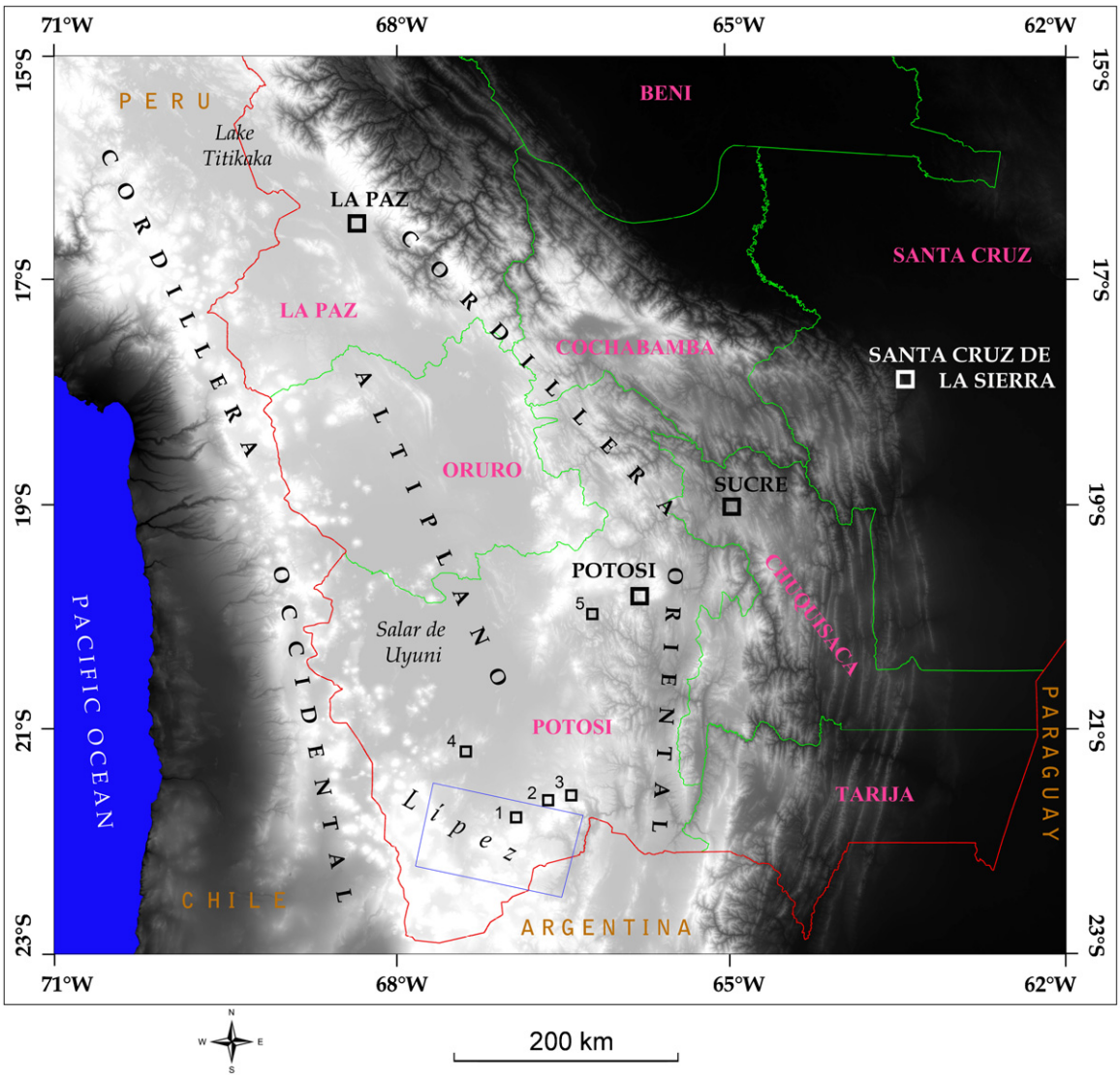


**Figure 1.** Location of the Lípez region in south Bolivia. Background: SRTM Digital Elevation Model (mosaicing of 12 1-degree square tiles). 3 arc-second resolution (∼90 m at the equator). White colour corresponds to elevation higher than 4500 m. Red lines: administrative boundary of Bolivia. Green lines: departmental boundary. The names of the Bolivian departments are given in pink capitals. The rectangle corresponds to the extent of the ALOS data (figure 2). Nos 1–5: mining places. (1) San Antonio de Lípez, (2) San Pablo de Lípez, (3) Santa Isabel, (4) San Cristobal and (5) Porco.

the south of San Antonio de Lípez, Cerro Lípez represents a large volume of Miocene dacites and rhyolites that intrude and overlie the ash-flow tuffs of the Upper Quehua Formation dated to about 16 Ma (Middle Miocene) (figure 2). Two calderas are present in the Sud Lípez. To the south of Cerro Lípez is the small Vilama caldera dated to 8.4 Ma (Soler *et al* 2007). To the southeast of Cerro Lípez, the large and Panizos caldera is dated between 6.8 and 7.9 Ma (Ort *et al* 1996). The last volcanic events in this area are those related to the Uturuncu dormant stratovolcano active between 890 and 271 ka (Sparks *et al* 2008) and to the Runtu Jarita dome rhyolitic intrusion dated to only 85 ka (Watts *et al* 1999). Different ignimbritic events occurred during the uppermost Tertiary and Quaternary times such as the Pastos Grandes Ignimbrite dated to 2.89 Ma (Upper Pliocene), the Laguna Colorada Ignimbrite dated to 1.98 Ma (lower Pleistocene) and the Tatio Ignimbrite dated to 0.7 Ma (middle Pleistocene) (Salisbury *et al* 2011). Active volcanoes are located further west on the border between Bolivia and Chile (Irruputuncu, Olca, Ollagüe, Putana, etc).

### *2.3. Historical and archaeological context*

The Sud Lípez area is the most inhospitable place of southern Bolivia. A rough climate and reduced vegetation made the setling of people hard. The exploitation of Cerro Lípez and the development of the San Antonio silver mines, represented at least by four separate mineralized systems, took place in this territory rich in ore deposits. The archaeological record consists of a high-altitude sanctuary at the top of Cerro Lípez, imperial Inca ceramic sherds at Wayco Seco and the ritual path. All these data reveal a first potential exploitation of the mineral deposit upon the arrival of the Spanish, which can be evidenced only by means of diligent excavation (Cruz *et al* 2012). Nevertheless, the Spanish period remains the most

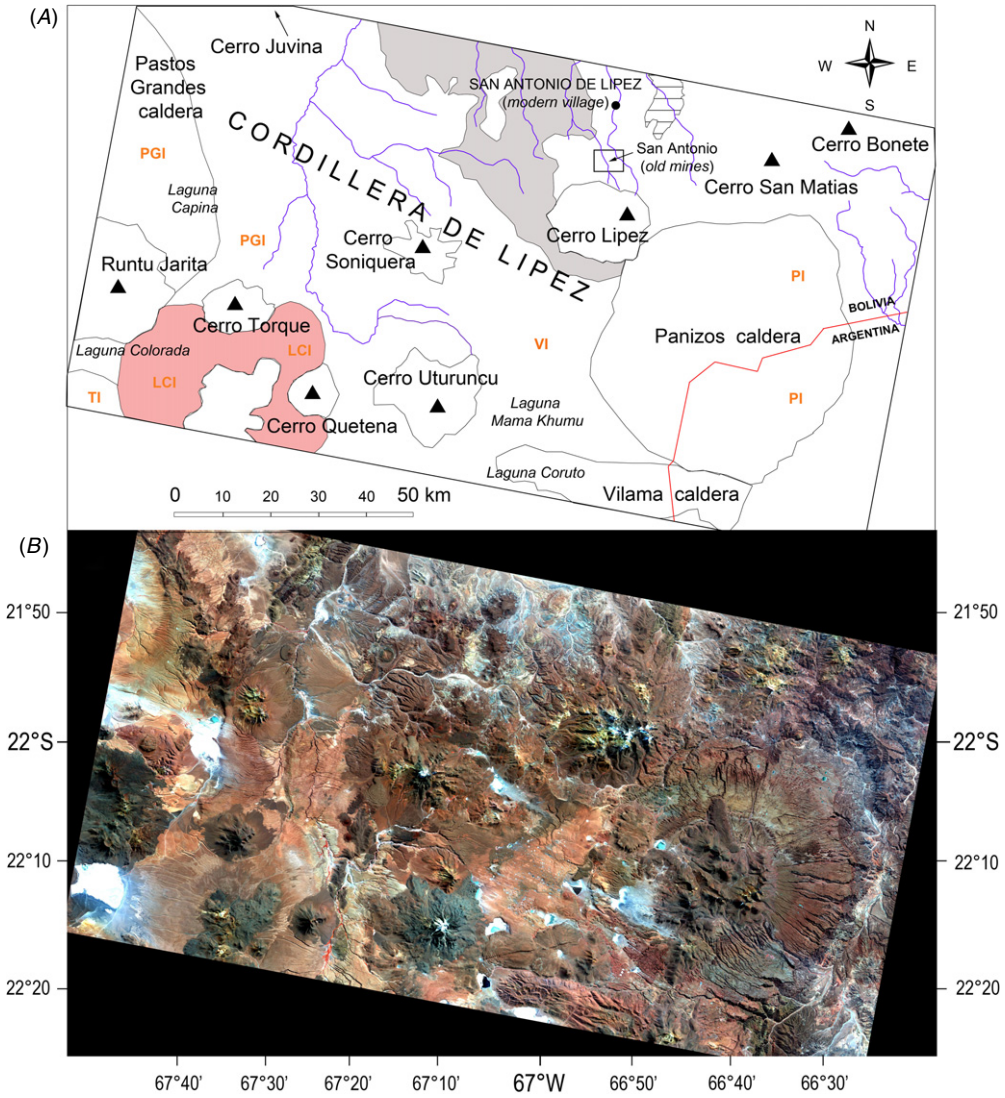


**Figure 2.** The Cordillera de Lípez. (*A*) Map of the main geological features. The rectangle showing the San Antonio old mines area corresponds to the extent of figures 4 and 5. LCI: Laguna Colorada Ignimbrite (in pink); PGI: Pastos Grandes Ignimbrite; PI: Panizos Ignimbrite; VI: Vilama Ignimbrite; Grey area: volcano-sedimentary deposits. (*B*) ALOS AVNIR-2 colour composite (red = band 4 near infrared range, green = band 2 green range, blue = band 2 blue range).

evident. According to Bakewell's work, the Spanish discovery of the deposit can be dated before 1640 (Bakewell 1988). In 1655, San Antonio knew its first mining boom, which was associated with a dramatic population growth in a zone where everything had to be imported to allow a sustainability of life (wood, fuel, food, tools, etc). The urban expansion, linked with the growth in mining activity continued until 1660. In 1664, the groundwater table was reached, and mining works were flooded. The activity declined until Lopes de Quiroga's arrival. The latter began the digging of a long adit that was finished in 1678 and led to the second mining boom of San Antonio de Lípez (1681–90). The ore deposit was then almost depleted. The 1725 census mentioned only 200 Indians in San Antonio. There were about 1000 in 1660. Whether or not the mine was abandoned, San Antonio remained a parish, as shown by the building of a church in 1800 and the still-active cemetery. Nevertheless, the place had no more urban or industrial character from the 18th century onward.

## 3. Material and methods

### *3.1. Remote-sensing data*

VHR could be defined for pixel size less than or equal to 2 m (figure 3). GeoEye-1 data with 0.5 m ground-pixel size was used in this study. Between 2 and 30 m, the spatial resolution is simply high, corresponding to one major advance with the launch of Landsat 4 in 1982. CBERS-2B (2.7 m), Spot 5-HRG (5 m/2.5 m) Alos-AVNIR-2 (10 m) and Landsat-TM (30 m) were the main sensors used. Between 30 and 100 m, the resolution is medium, including the first digital images from Landsat 1 (1972) with 79 m pixel size. Between 100 and 1000 m, the resolution is low or moderate, and very low beyond 1000 m (geostationary satellites only). The latter were not used for this study.

*3.1.1. Corona.* The Corona programme was a series of more than 100 American strategic reconnaissance satellites operated

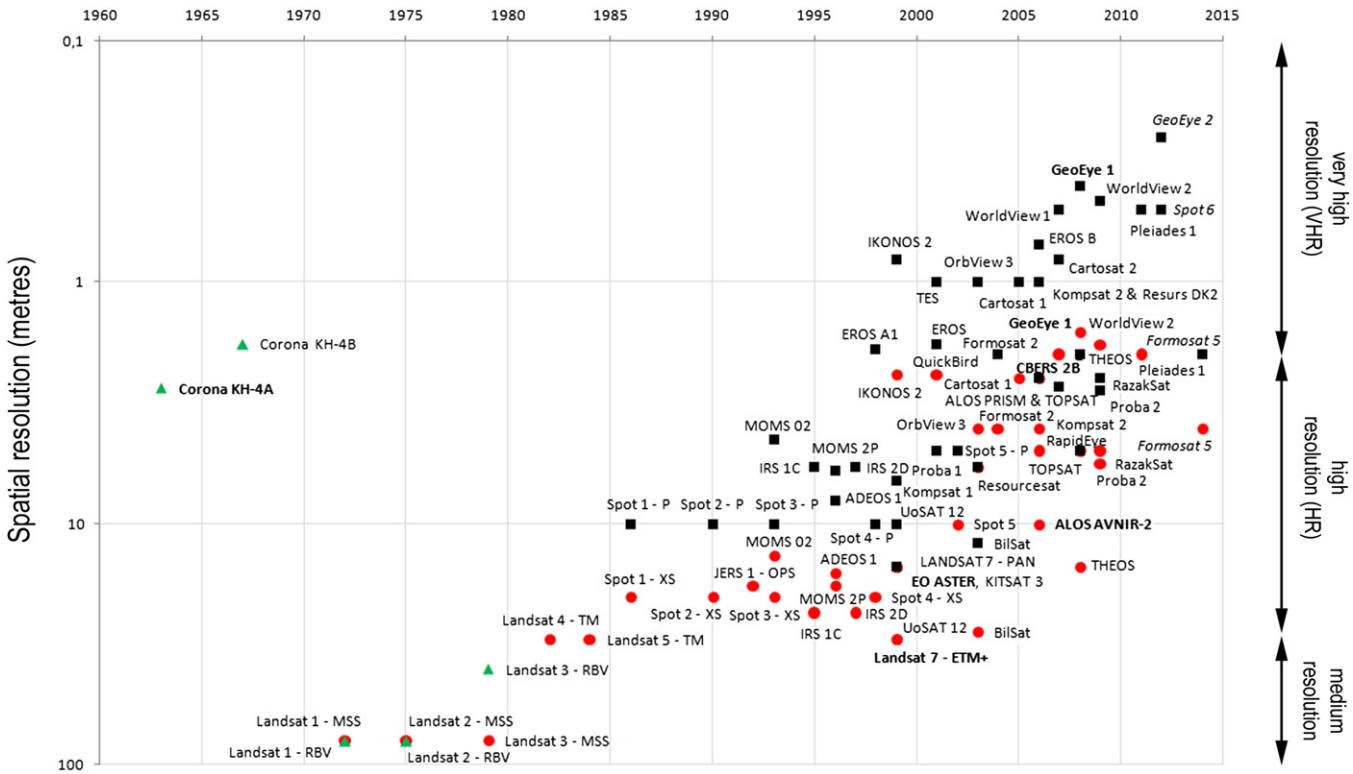


**Figure 3.** The improvement of the spatial resolution of the remote sensing instruments. Black squares: panchromatic sensors. Red dots: multispectral sensors. Green triangles: photographic process. Sensors to be launched are indicated in italics. Sensors used in the present study are indicated in bold.

by the Central Intelligence Agency Directorate of Science and Technology with the assistance of the US Air Force. The Corona satellites were firstly used for the photographic surveillance of the Soviet Union, the People's Republic of China, and other areas beginning in June 1959 and ending in May 1972. In this work we use the so-called no DS1026-1014DF065 dataset acquired on 29 October 1965 by the KH-4A camera onboard Corona J-1 launched from Vandenberg Air Force Base the day before. The KH-4A camera was capable of acquiring photographic data at 2.75 m panchromatic resolution with important geometric deformation on the image data.

*3.1.2. Landsat.* The Landsat system is the longest running programme for acquiring imagery of the Earth's surface from space. Landsat 1 was launched in July 1972. The most recent, Landsat 7, was launched in April 1999. The different instruments onboard Landsat satellites have acquired millions of images, forming a unique archive. In this study, we use numerous Landsat scenes, including the scene (Path: 232; Row:075) acquired on 1 May 2005 with the Thematic Mapper sensor onboard Landsat 5 launched on 1 March 1984 and still active.

*3.1.3. Spot 5.* SPOT 5 is operated by the French Space Agency (CNES). It was launched on 4 May 2002. SPOT 5 has two high resolution geometrical (HRG) instruments. They offer a resolution of 2.5 to 5 m in panchromatic mode and 10 m in multispectral mode. The next SPOT satellite, SPOT 6, is expected to be launched in 2012. It will allow acquisition of panchromatic images with 1.5 m resolution. In this study, we use the Spot 5 data available in Google Earth only in true colour composite. The image was acquired on 18 May 2004.

*3.1.4. CBERS.* The China–Brazil Earth Resources Satellite programme (CBERS) is a technological cooperation programme between Brazil and China which has been developing and operating Earth observation satellites since 1999. The last operational satellite, the so-called CBERS-2B, was launched on 19 September 2007 from the Taiyuan base in China. The satellite operated until 10 May 2010. CBERS-2B carried four remote-sensing instruments, including the Wide Field Imager Camera, the Medium Resolution Camera and the Infrared Multispectral Scanner Camera. The main CBERS-2B's instrument was the High Resolution Panchromatic Camera (HRC). This camera records images in one single panchromatic band, with 27 km width and 2.7 m spatial resolution. Three HRC images are available on the San Antonio de Lípez test site acquired on 5 May 2008, 6 October 2009 and 15 January 2010, respectively.

*3.1.5. ALOS.* The Japanese Advanced Land Observation Satellite (ALOS) was launched on 24 January 2006 from the Tanegashima Space Center. It was declared dead in orbit on 12 May 2011, after abruptly powering down on 22 April, that is, all of its on-board observation devices were turned off. ALOS was the largest satellite developed in Japan. It carried three remote-sensing instruments: the Phased Array

**Table 1.** Main spatial and spectral characteristics of the remote sensing data.

| Sensor satellite | Panchromatic | Visible | NIR | MIR | SWIR |
|---|---|---|---|---|---|
| | Range | | | | |
| | 0.5–0.9 $\mu$m | 0.4–0.7 $\mu$m | 0.7–0.9 $\mu$m | 1.55–1.75 $\mu$m | 2.1–2.5 $\mu$m |
| KH 4A-Corona | 2.75 m | NA | NA | NA | NA |
| GeoEye 1 | 0.41 m | 1.64 m | 1.64 m | NA | NA |
| HRC CBERS-2B | 2.7 m | NA | NA | NA | NA |
| HRG SPOT 5 | 5 m | 10 m | 10 m | 20 m | NA |
| AVNIR-2 ALOS | NA | 10 m | 10 m | NA | NA |
| Aster-EO[a] | NA | 15 m | 15 m | 30 m | 30 m |
| XS-SPOT 1–3[a] | 10 m | 20 m | 20 m | NA | NA |
| ETM+ Landsat[a] | 15 m | 30 m | 30 m | 30 m | 30 m |
| TM Landsat 4–5 | NA | 30 m | 30 m | 30 m | 30 m |
| MSS Landsat[a] | NA | 79 m | 79 m | NA | NA |

[a] Sensor not illustrated in this study. NA: band not available.

L-band Synthetic Aperture Radar (PALSAR), the Panchromatic Remote-Sensing Instrument for Stereo Mapping (PRISM) and the multispectral Advanced Visible and Near-Infrared Radiometer type 2 (AVNIR-2). In this study we use an AVNIR-2 scene with 10 m spatial resolution acquired on 30 May 2009, in the frame of the pilot-project 'Geological Mapping of Sensitive Environments' supported by the Japanese Space Agency (JAXA) and the European Space Agency (ESA).

*3.1.6. GeoEye-1.* The GeoEye-1 satellite sensor, formerly known as OrbView-5, was launched on 6 September 2008 from Vandenberg Air Force Base. It features the most sophisticated technology ever used in a civilian remote-sensing system and provides 41 cm panchromatic and 1.65 m multispectral imagery in 15.2 km swaths. GeoEye-2, expected to be launched in 2012 (figure 2), will provide 25 cm panchromatic imagery, but for military use only.

The instrument is highly pointable (up to $\pm 60^{\circ}$) in the cross-track direction. Thus, a scene was ordered and acquired on 24 March 2011, a few days before the last field mission.

### *3.2. Methodology used*

Corona satellite photography has already been applied in archaeological survey projects (Goossens *et al* 2006). However, the imagery is difficult to process because of great conical distortion. Some Corona sensors produce a forward and an afterward image of the same area with a different viewing angle for stereoscopy. This characteristic is not available for our site. The photography is then interpreted such as an aerial photograph.

Digitally processed satellite data were necessary as a tool in detecting geological and archaeological features. Different colour composites were created according to the spatial and spectral characteristics of each sensor (table 1). Data registration was needed to reference images to geographic coordinates (UTM in our case) and to correct them to match base image geometry.

The Landsat Thematic Mapper calibration was used for studying lithologies. Landsat TM calibration converts digital numbers to exoatmospheric reflectance. Due to the great purity of the local atmosphere (and the lack of any detailed meteorological data), the exoatmospheric reflectance is highly related to the surface reflectance. The exoatmospheric reflectance ($\rho$) is calculated using the following equation:

$$\rho = (\pi . L_{\lambda} . d^2)/E_{\mathrm{SUN}} . \cos \Theta$$

where $L_{\lambda}$ is the spectral radiance, $d$ is the Earth–Sun distance in astronomical units, $E_{\mathrm{SUN}}$ is the mean solar exoatmospheric irradiance and $\theta$ is the solar zenith angle expressed in degrees. $E_{\mathrm{SUN}}$ is derived from tables provided in the Landsat technical notes. The reflectance is expressed in decimal (e.g. 0.210) or in percentage (e.g. 21%).

Colour GeoEye-1 imagery was created using a pan-sharpening process that combines the high-resolution panchromatic image with the multispectral bands to create a 0.5 m colour product including four bands (blue, green, red, near infrared).

## 4. Results

### *4.1. Geological framework*

ALOS-AVNIR-2 is able to point out the main geological features. Figure 2 illustrates the main volcanoes of the area along with the associated ignimbrites (deposition from a pumiceous pyroclastic flow) and some volcano-sedimentary deposits (see the grey colour in the west of Cerro Lípez and to the north). The most recent ignimbrites (Laguna Colorada and Pastos Grandes Ignimbrites) are highly textured, whereas the oldest ignimbrites are smoother and suffer more drastically the glacial influence. The presence of the large Lípez WNW-ESE lineament should also be noted. This lineament is revealed by a number of modern rivers elongated according to its main direction. The Lípez lineament is detectable between Pastos Grandes Caldera and Panizos Caldera.

In spite of its high spatial resolution, ALOS-AVNIR-2 offers a limited spectral range and, thus, cannot be used for detailed spectral studies. Therefore, Landsat Thematic Mapper data were used for extracting the reflectance of the different lithological units: stocks/plugs, lava flows, ignimbrites, volcano-sedimentary deposits, hydrothermally altered rocks, exploration areas, etc (figure 4 and table 2).

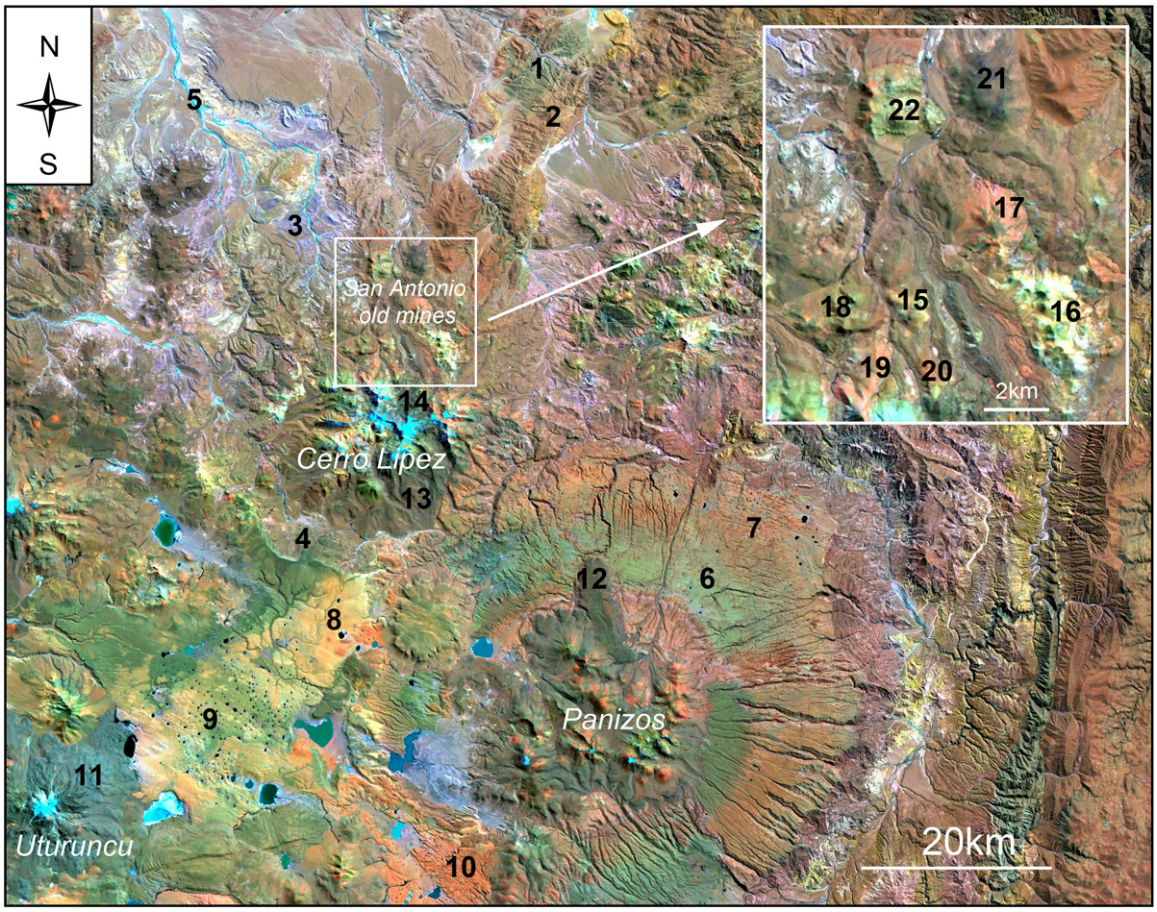


**Figure 4.** Location of the 22 regions of interest (see also table 2). The background is the Landsat TM image acquired on 1 May 2005 (red = band 7 SWIR range, green = band 3 red range, blue = band 1 blue range).

Each region of interest (nos 1–22) comprises 1000 to 20 000 pixels, corresponding to 90ha to 1800ha, respectively.

Concerning the lava flows, the high reflectance of the Vilama Caldera in the mid-infrared (MIR) (0.289 ± 0.054) and short-wave infrared (SWIR) (0.305 ± 0.057) ranges (table 2, no 10) should be emphasized. This flow is andesitic in nature and relatively less viscous than the rhyolite-dacite flows (for example Uturuncu, no 11). MIR and SWIR ranges allow the distinguishing of the different ignimbrites related to the Panizos and Vilama Calderas. Generally, ignimbrites show higher reflectance in the IR range than the lavas. Reflectance values are relatively similar for ignimbrites and volcano-sedimentary rocks, as illustrated by no 6 (Panizos Ignimbrite) and no 4 (volcano-sedimentary deposits around the Cerro Lípez).

In the San Antonio mining zone, different dacite-rhyolite domes show relatively different reflectance (see for example, nos 16–20). Quebrada East (no 16) shows high IR reflectance and corresponds to altered dacite with mineralization. The peak in the red range (0.238 ± 0.055) could correspond to the wealth of iron oxides. The main mineralized zone (no 15), the so-called Mesa de Plata (*the silver table*), has now a very complex surface and its reflectance is highly influenced by old works, modern pitting, etc. Nevertheless, the main hydrothermal alteration zone is clearly visible, even in the visible range (i.e. in the field).

It should be mentioned that the field work has also demonstrated the influence of the glacial dynamics. Moraine deposits were left by valley glaciers developed in the past. This has great spectral and textural effects and deeply influences the development of the vegetation.

### *4.2. Recent mining works (since the 1960s)*

Figures 5 and 6 present the Corona image and the GeoEye-1 false colour composite, respectively. There is a great difference between those two images illustrating the area of the old San Antonio mines. Corona was acquired in October, whereas GeoEye was acquired in March. The GeoEye colour composite points out the vegetation areas that appear in red because of the high reflectance in the near-infrared radiation. This is clearly the case for zones of cushion vegetation along the river downstream Asiento. Corona shows black places corresponding to water: small lakes (SW Asiento, no 1), the flooded border of the river (north, no 2), the Rio de los Ingenios close to the Quebrada (no 3) which is larger than that in the March image (seasonal effect).

There are also differences in the tracks. A small track starting from the right bank of the Rio de los Ingenios is visible in the Corona image (no 4). It corresponds to exploration carried out in the late 1950s–early 1960s. Now this path is almost abandoned. The same kind of feature appears to the south of Asiento (no 5).

**Table 2.** Landsat TM calibrated Reflectance (mean and standard deviation) of some regions of interest (see figure 4 for location).

| | Band 1 Blue | Band 2 Green | Band 3 Red | Band 4 near IR | Band 5 mid IR | Band 7 SWIR |
|---|---|---|---|---|---|---|
| Sedimentary | | | | | | |
| 1. Ordovician North-West | 0.118 ± 0.011 | 0.145 ± 0.019 | 0.170 ± 0.026 | 0.204 ± 0.034 | 0.235 ± 0.044 | 0.219 ± 0.041 |
| 2. Ordovician South | 0.116 ± 0.010 | 0.142 ± 0.019 | 0.169 ± 0.025 | 0.212 ± 0.033 | 0.281 ± 0.044 | 0.261 ± 0.042 |
| 3. VS (Upper Quehua) | 0.155 ± 0.030 | 0.170 ± 0.032 | 0.186 ± 0.033 | 0.210 ± 0.037 | 0.210 ± 0.034 | 0.222 ± 0.034 |
| 4. VS (around Cerro Lipez) | 0.128 ± 0.016 | 0.149 ± 0.019 | 0.180 ± 0.022 | 0.219 ± 0.024 | 0.227 ± 0.034 | 0.233 ± 0.037 |
| 5. Alluvials (north) | 0.179 ± 0.029 | 0.199 ± 0.029 | 0.226 ± 0.030 | 0.258 ± 0.034 | 0.243 ± 0.045 | 0.238 ± 0.068 |
| Ignimbrites | | | | | | |
| 6. Panizos IG (upper part) | 0.124 ± 0.010 | 0.151 ± 0.015 | 0.188 ± 0.020 | 0.221 ± 0.023 | 0.220 ± 0.025 | 0.228 ± 0.027 |
| 7. Panizos IG (lower part) | 0.115 ± 0.009 | 0.132 ± 0.014 | 0.165 ± 0.019 | 0.211 ± 0.024 | 0.254 ± 0.032 | 0.272 ± 0.034 |
| 8. Vilama IG (north) | 0.120 ± 0.006 | 0.151 ± 0.009 | 0.212 ± 0.013 | 0.270 ± 0.016 | 0.330 ± 0.020 | 0.334 ± 0.020 |
| 9. Vilama IG (south) | 0.122 ± 0.012 | 0.149 ± 0.017 | 0.204 ± 0.030 | 0.246 ± 0.046 | 0.268 ± 0.063 | 0.272 ± 0.062 |
| Stocks and flows | | | | | | |
| 10. Vilama Caldera | 0.103 ± 0.009 | 0.115 ± 0.015 | 0.152 ± 0.023 | 0.195 ± 0.033 | 0.289 ± 0.054 | 0.305 ± 0.057 |
| 11. Uturuncu Dome | 0.133 ± 0.001 | 0.151 ± 0.014 | 0.177 ± 0.017 | 0.194 ± 0.022 | 0.170 ± 0.025 | 0.167 ± 0.023 |
| 12. Panizos (north flow) | 0.103 ± 0.004 | 0.114 ± 0.006 | 0.137 ± 0.008 | 0.167 ± 0.012 | 0.175 ± 0.020 | 0.167 ± 0.018 |
| 13. Lipez (south face) | 0.107 ± 0.010 | 0.119 ± 0.014 | 0.141 ± 0.017 | 0.177 ± 0.026 | 0.190 ± 0.031 | 0.182 ± 0.031 |
| 14. Lipez (north face) | 0.112 ± 0.025 | 0.122 ± 0.028 | 0.143 ± 0.032 | 0.165 ± 0.040 | 0.148 ± 0.040 | 0.148 ± 0.037 |
| Mining zone | | | | | | |
| 15. Mesa de Plata | 0.122 ± 0.015 | 0.152 ± 0.028 | 0.195 ± 0.041 | 0.244 ± 0.050 | 0.293 ± 0.074 | 0.264 ± 0.063 |
| 16. Quebrada East | 0.142 ± 0.026 | 0.186 ± 0.042 | 0.238 ± 0.055 | 0.283 ± 0.065 | 0.325 ± 0.089 | 0.303 ± 0.075 |
| 17. Quebrada North East | 0.128 ± 0.012 | 0.149 ± 0.014 | 0.187 ± 0.020 | 0.249 ± 0.025 | 0.331 ± 0.062 | 0.325 ± 0.065 |
| 18. Pavilion West | 0.113 ± 0.013 | 0.137 ± 0.021 | 0.175 ± 0.029 | 0.220 ± 0.042 | 0.229 ± 0.049 | 0.232 ± 0.048 |
| 19. Asiento upstream | 0.125 ± 0.010 | 0.150 ± 0.014 | 0.192 ± 0.019 | 0.241 ± 0.024 | 0.303 ± 0.050 | 0.314 ± 0.054 |
| 20. Small dome (south) | 0.110 ± 0.012 | 0.127 ± 0.017 | 0.165 ± 0.023 | 0.209 ± 0.036 | 0.283 ± 0.062 | 0.290 ± 0.060 |
| 21. Black mount (north) | 0.106 ± 0.010 | 0.114 ± 0.014 | 0.132 ± 0.018 | 0.168 ± 0.030 | 0.172 ± 0.038 | 0.163 ± 0.037 |
| 22. Intrusion (north) | 0.126 ± 0.017 | 0.158 ± 0.027 | 0.200 ± 0.036 | 0.248 ± 0.048 | 0.247 ± 0.054 | 0.247 ± 0.056 |

The main pits, north–south oriented, have been drilled above the Mesa de Plata ore deposit between 1965 and 2005. We explored a set of Landsat data (MSS, TM and ETM+) in order to date the exploration phases. Unfortunately, the main pits dated before 1982 and no high resolution data are available. Landsat MSS with its 79 m pixel size is not capable of distinguishing the pits which are about 6 m large. These pits could have been done in 1981–82 during the last important COMIBOL (the Bolivian mining company) exploration.

### *4.3. Mapping the archaeological remains*

The archaeological area can be bounded in different spaces. Asiento and Wayco Seco are separated by the Mesa de Plata ore deposit, where the major part of the mining entrances is situated. The Quebrada de los Ingenios in the northeast and the Cerro Lípez in the south are also the places of archaeological discoveries. The surface covers a total of several square kilometres. We tried to estimate the urban evolution linked to the mining setting-up in the San Antonio area using the VHR GeoEye-1 data analysis supplemented by field checking. At the end, we obtain a correctly georeferenced general map containing information of the same level but acquired in two different ways. The whole operation is carried out in five days of field investigation by two persons.

In the south, the atlas of the site is drawn to have a foreground which will serve as a source document in the field. According to our technical choice we favour elements, the reading of which is sure in order to limit over-interpretation. This one is a factor of slowing down of the survey because it obliges the archaeologist to look for non-existing structures, introducing every time doubt in their mind. On-site, the map is corrected and information such as architectural elements (door, niche and window), elements of town planning (path network, paved yard) and the characterization of buildings (chapels, cemeteries, industrial buildings, mining entrances etc) is added. Figure 7 illustrates the results for two sectors located in Wayco Seco and Asiento, respectively.

## 5. Discussion

### *5.1. Data registration and digital analysis*

Classically used in geological remote sensing, satellite data appeared to be of great interest for mapping the lithological units of the Lípez region. In this study, the high altitude (>4500 m) and the pure atmosphere allowed a spectral approach without intensive field spectrometry. The geomorphological, geological, mineral and archaeological analysis of the area was deeply helped by the use of satellite images including panchromatic images (CBERS-2B), multispectral high resolution data (Spot 5), multispectral with large radiometric range (Landsat TM) and very high multispectral data (GeoEye-1). The detailed geological mapping is still in development and will be published elsewhere.

We have shown that archived Corona KH-4A images are valuable instruments to produce the image of the studied area almost half a century before our field investigation. With the set of georeferenced (except Corona) documents at the pixel level,

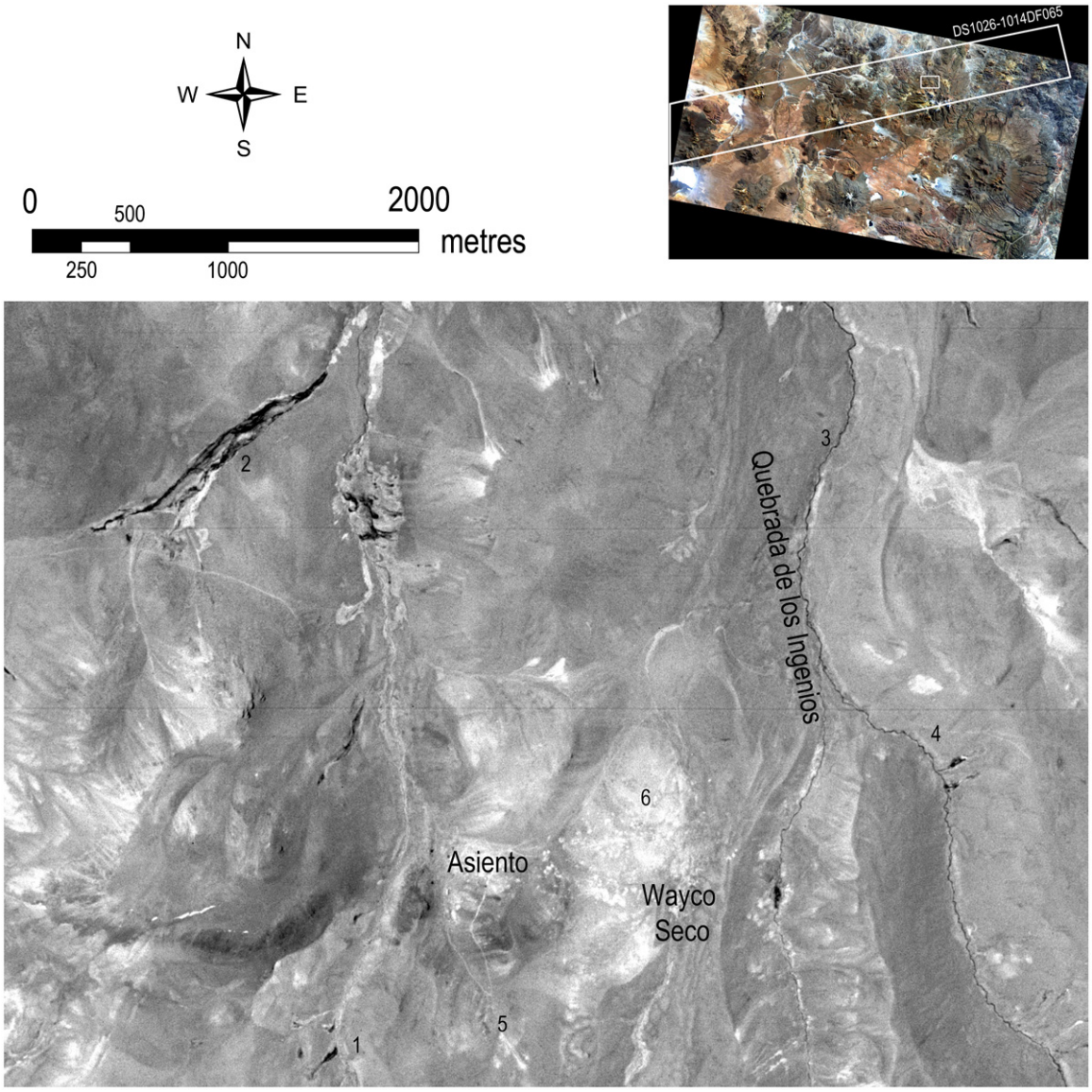


**Figure 5.** The San Antonio mining area viewed by Corona on 26 October 1965. The track of the Corona data is indicated in the upper-right corner. The small rectangle inside the track corresponds to the extent of the subimage. Geographical coordinates are not indicated because the Corona data suffer important geometric deformation (conical distortion).

it is possible to go into a detailed analysis of the landscape features (pointing out the role of the glacial dynamics), the geological context and the related archaeological sites. As a last illustration, figure 8 shows the comparison of Corona, CBERS-2B, Spot 5 and Geo-Eye-1 on the area of Mesa de Plata. The inset shows the enlargement of Asiento (ruins) and illustrates the major step due to the VHR remote sensing. We have already shown that a resolution $\leqslant 0.75$ m is necessary for archaeological investigations (Deroin *et al* 2011). GeoEye-1 (0.41 m), WorldView-2 (0.46 m), WorldView-1 (0.50 m), QuickBird (0.61 m), EROS-B −0.70 m) and the recently launched Pleiades (0.70 m) are currently the only satellites with this requirement.

### *5.2. The archaeological survey*

This is the first time that the satellite image has been at the origin of the feasibility of an archaeological operation within the framework of a surveying inventory. Thus, we also looked for the quality of the information collected before its use. With this aim, we compared the built elements remotely sensed on the GeoEye image with what we observed in the field. A simple work with classical image processing software along with the visual interpretation of the colour composite allows measuring the surface covered by walls drawn according to the image, added and deducted during the survey. We obtained rates expressed in the percentage of pixels representing: the percentage of walls identified in the image and validated in the field, the percentage of over-interpretation and the percentage concerning the unrevealed elements (table 3). Although all the buildings were studied, we present only two plates in this paper representing Asiento and Wayco Seco. The difference of preservation between these two settlements which enclose Mesa de Plata allows qualifying of the efficiency of the photographic study. In the case of Asiento, nearly

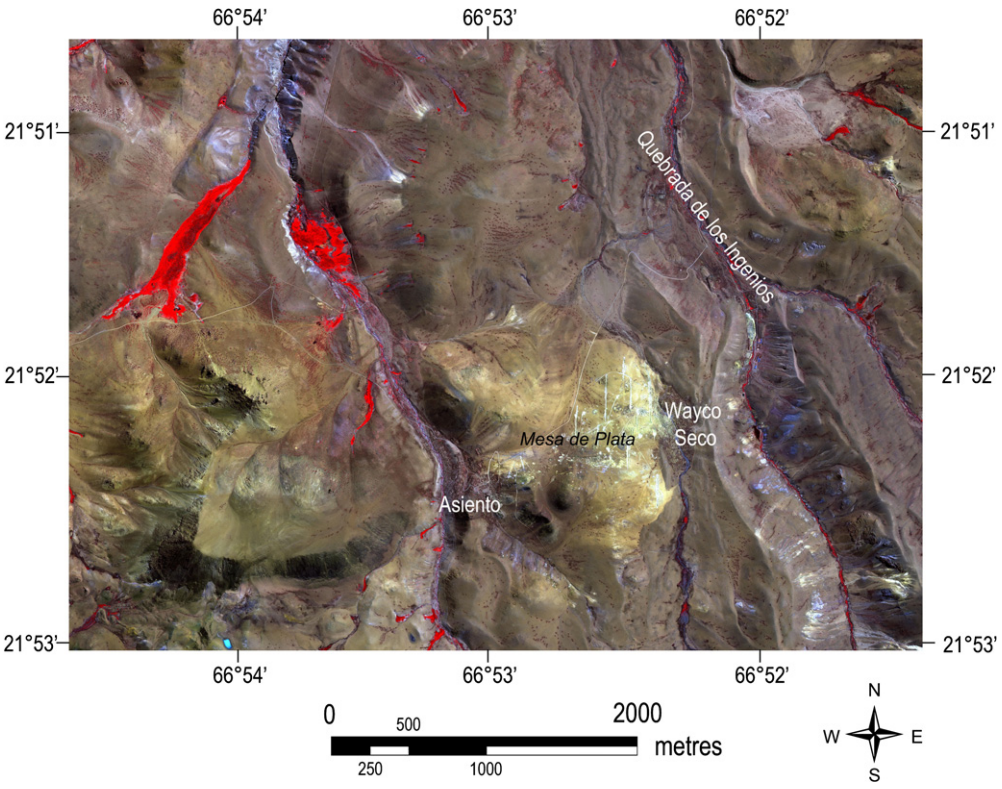


**Figure 6.** A recent view of the San Antonio mining area. GeoEye-1 acquired on 24 March 2011. Colour composite: red = near infrared range; green = red range; blue = blue range).

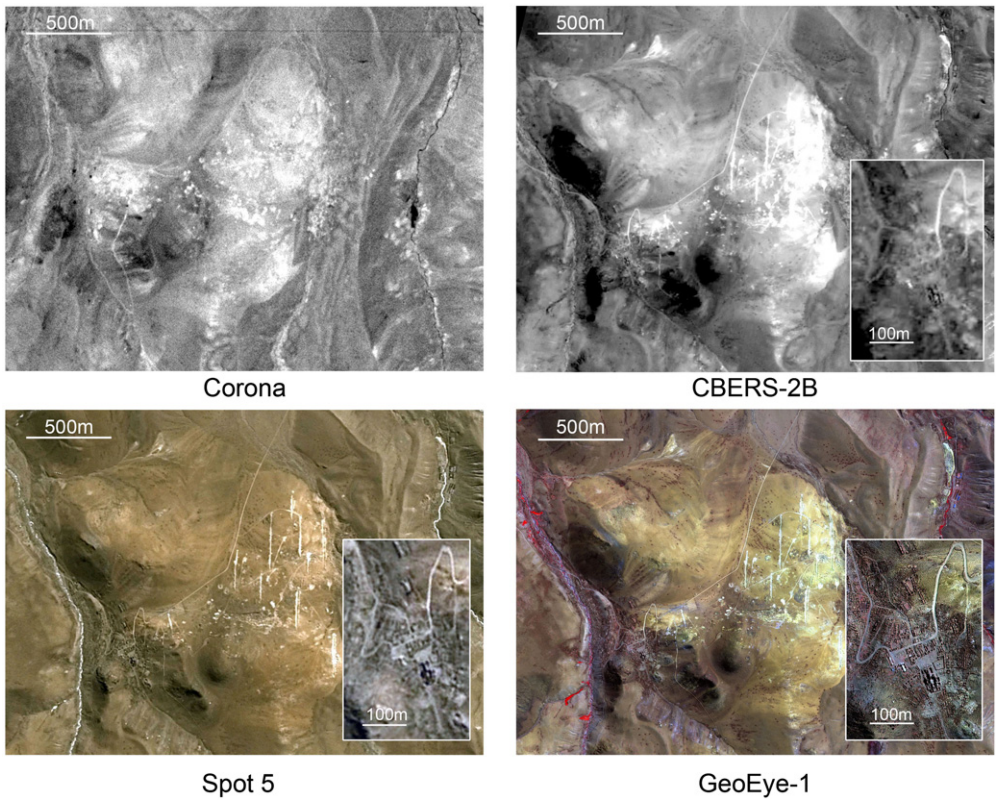


**Figure 7.** Cartography of the archaeological remains in two areas: Asiento and Wayco Seco.

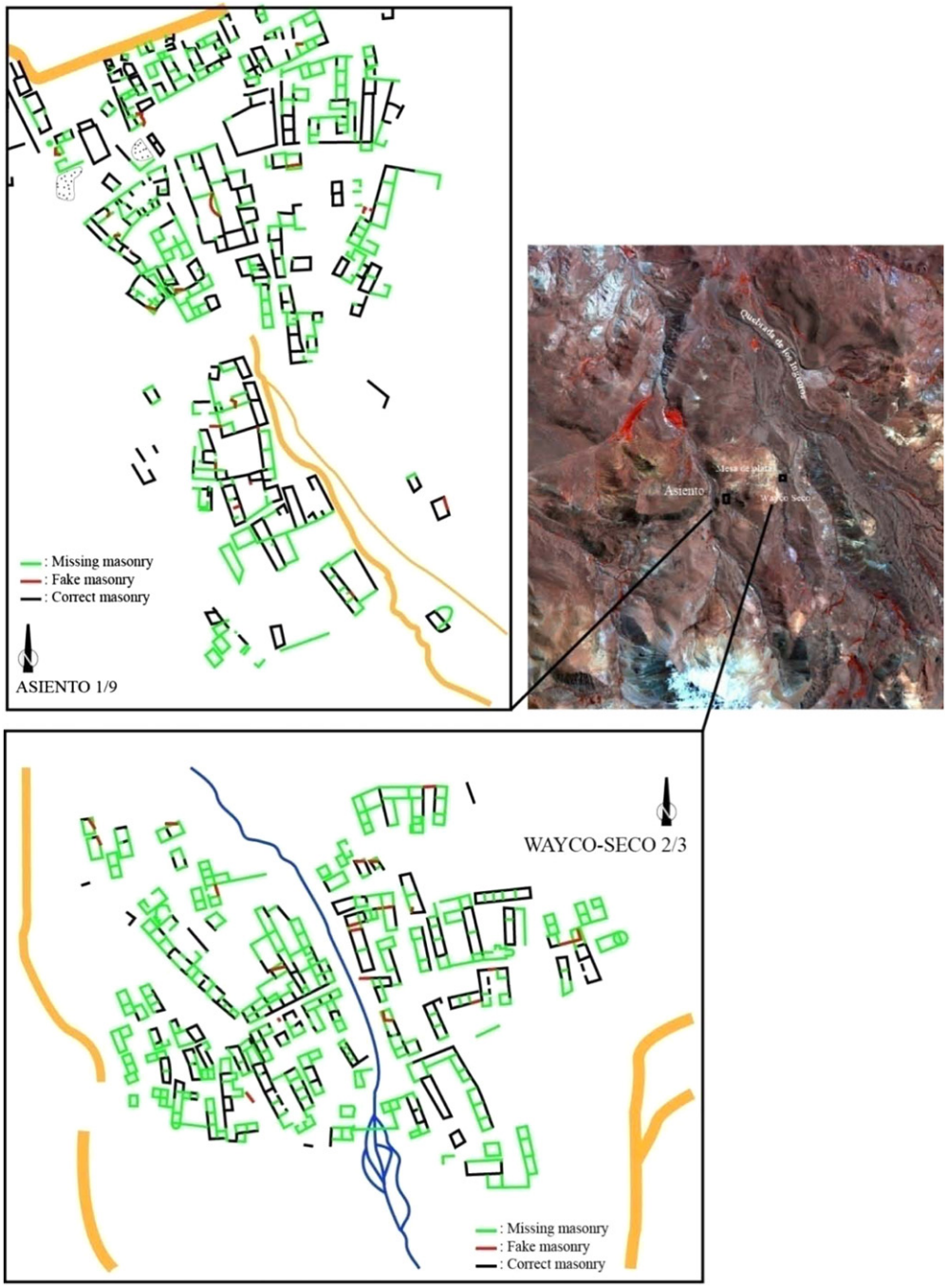


**Figure 8.** Comparison of four remote sensing data on the San Antonio de Lípez test site. The enlargement (lower-right corner) corresponds to Asiento.

**Table 3.** Evaluation of the GeoEye-1's accuracy for the detailed mapping of the archaeological remains.

| | Asiento 1/9 | Wayco seco 2/3 |
|---|---|---|
| Correct masonry | 62.5% | 33.5% |
| Fake masonry | 2.2% | 2.1% |
| Missing masonry | 35.3% | 64.4% |

two-thirds of buildings are spotted in the image, while only one-third is identified in Wayco Seco. These two settlements date back approximately to the same period. Asiento represents the town where the Spanish settled down, while Wayco Seco is a slightly older place. During the digging of the drainage adit, Quiroga was forced to give up the 'rancherias' of Wayco Seco. Indeed, these installations overstand numerous mining entrances. According to Quiroga's statement, they were used by 'kajchas' (thieves of ore). This reduced the advantage of the adit designed to slope slightly upwards from the entrance, so that water flowed freely out of the mine. Indeed, it seems that the drainage adit was dug between 1676 and 1678.

If the rate of valid construction is widely variable from one set to the other because of identified historical reasons, the percentage of errors remains low and identical: overinterpretation is thus almost absent. The consequence is a

relatively high rate of unrevealed elements. Lowering this rate is probably not interesting, because it will increase errors and, therefore, conduct more difficult field work.

The field survey is vital at least to qualify observed elements. The preliminary processing of the satellite image allowed us to cover a large area including 46 mining entrances, 58 industrial buildings and 6 places of worship. It becomes possible after an image recovery to quantify the surface of the industrial installations. We shall be interested in particular in the surface of patio within the ore dressing units. The work is practicable in the field, but is time consuming. The wealth of this approach within the framework of archaeological survey is real, and we shall develop it for other deserted zones.

## 6. Conclusion

Results from our geoarchaeological study in southernmost Bolivia pointed out that the GeoEye-1 data, captured at 0.41 m nadir resolution and resampled to 0.5 m, constitute a powerful tool for mapping the archaeological records. Panchromatic data (CBERS-2B, Landsat ETM+, etc) are also interesting, but only the VHR associated with the multispectral character of the sensor (pan-sharpening) allows detailed mapping.

We hope to have demonstrated that archive satellite images, especially Corona KH-4A, are valuable instruments to produce a series of documents for topographical and geomorphological purposes. These images along with the numerous multispectral high-resolution data (Landsat TM, Spot 5, etc) render it possible to go into a detailed analysis of the landscape features and the related archaeological sites. This also emphasizes the importance of the data integration including data registration.

Further progress in geoarchaeological mapping will need better resolution than 0.50 m. Whilst satellite resolutions continue to improve, the distribution of VHR imagery from satellites at better than 0.50 m is subjected to prior approval by the US Government. Without this approval, images at resolutions better than 0.5 m will be resampled to give 0.5 m resolution, such as our own GeoEye-1 scene.

## Acknowledgment

We thank the French-Argentine ECOS-SUD project for funding some of the field missions carried out in the framework of this cooperative work.

## References

Ahlfeld F 1967 Metallogenetic epochs and provinces of Bolivia. The Tin-Province: part I. The metallogenetic provinces of the Altiplano: part II *Mineralium Depos.* **2** 291–311

Baker M C W 1981 The nature and distribution of upper cenozoic ignimbrite centres in the Central Andes *J. Volcanol. Geotherm. Res.* **11** 293–315

Bakewell P 1988 *Silver and Entrepreneurship in the Seventeenth Century Potosi, the Life and Times of Antonio Lopez de Quiroga* (New Mexico: University of New Mexico Press) pp 1–250

Cáceres F, Bonino E and Pirard E 2004 Teledetección geológica de la region de San Pablo de Lipez—Bolivia *Congr. Geol. Bol.* **100** 496–505

Cruz P, Nielsen A, Téreygeol F, Deroin J P and Guillot I 2012 La pacificación del mineral. Cerro Lípez, un enclave minero en la contienda sobre el Nuevo Mundo *Vestigios–Revista Latinoamericana de Arqueología Histórica* at press

de Silva L S and Gosnold W D 2007 Episodic construction of batholiths: insights from the spatiotemporal development of an ignimbrite flare-up *J. Volcanol. Geotherm. Res.* **167** 320–35

Deroin J P, Téreygeol F and Heckes J 2011 Evaluation of very high to medium resolution multispectral satellite imagery for geoarchaeology in arid regions, case study from Jabali, Yemen *J. Archaeological Sci.* **38** 101–14

Deroin J P, Téreygeol F and Heckes J 2012 Remote sensing study of the ancient Jabali silver mines (Yemen): from past to present *Remote Sensing and Digital Image Processing 16 Satellite Remote Sensing, Part 3* ed R Lasaponara and N Masini (Berlin: Springer) pp 231–45

El Shazly E M, Abdel Hady M A and El Nasharty F A 1988 Gold exploration by remote sensing techniques in the Wadi El Allaqi area, Egypt *Photogrammetria* **42** 303–10

Francis P W and Baker M C W 1978 Sources of two large ignimbrites in the central Andes: some Landsat evidence *J. Volcanol. Geotherm. Res.* **4** 81–87

Francis P W, Halls C and Baker M C W 1983 Relationships between mineralization and silicic volcanism in the Central Andes *J. Volcanol. Geotherm. Res.* **18** 165–90

Garrison T G, Houston S D, Golden C and Inomata T 2008 Evaluation the use of IKONOS satellite imagery in lowland Maya settlement archaeology *J. Archaeological Sci.* **35** 2770–7

Goossens R, De Wulf A, Bourgeois J, Gheyle W and Willems T 2006 Satellite imagery and archaeology: the example of CORONA in the Altai Mountains *J. Archaeol. Sci.* **33** 745–55

Hérail G, Oiler J, Baby P, Bonhomme M and Soler P 1996 Strike-slip faulting, thrusting and related basins in the Cenozoic evolution of the southern branch of the Bolivian Orocline *Tectonophysics* **259** 201–12

Kay S M, Coira B L, Caffe P J and Chen C-H 2010 Regional chemical diversity, crustal and mantle sources and evolution of central Andean Puna plateau ignimbrites *J. Volcanol. Geotherm. Res.* **198** 81–111

Kussmaul S, Hörmann P K, Ploskonka E and Subieta T 1977 Volcanism and structure of southwestern Bolivia *J. Volcanol. Geotherm. Res.* **2** 73–111

Lasaponara R, Coluzzi R, Gizzi F T and Masini N 2010 On the LiDAR contribution for the archaeological and geomorphological study of a deserted medieval village in Southern Italy *J. Geophys. Eng.* **7** 155–63

Lasaponara R and Masini N 2011 Satellite remote sensing in archaeology: past, present and future perspectives *J. Archaeological Sci.* **38** 1995–2002

Lasaponara R and Masini N (eds) 2012 Satellite Remote Sensing. A New Tool for Archaeology *(Series Remote Sensing and Digital Image Processing* vol 16*)* (Berlin: Springer) pp 1–364

Masini N and Soldovieri F 2011 Integrated non-invasive sensing techniques and geophysical methods for the study and conservation of architectural, archaeological and artistic heritage *J. Geophys. Eng.* **8** doi:10.1088/1742-2132/8/3/E01

Matteini M, Mazzuoli R, Omarini R, Cas R and Maas R 2002 Geodynamical evolution of Central Andes at 24°S as inferred by magma composition along the Calama–Olacapato–El Toro transversal volcanic belt *J. Volcanol. Geotherm. Res.* **118** 205–28

Ort M H, Coira B L and Mazzoni M M 1996 Generation of a crust-mantle magma mixture: magma sources and contamination at Cerro Panizos, central Andes *Contrib. Mineral. Petrol.* **123** 308–22

Petersen G P 2010 Mining and metallurgy in ancient Perú. A translation of Minería en el Antiguo Perú by W E Brooks *Geol. Soc. Am. Spec. Paper* **467** 1–90

Phillipson S E and Romberger S B 2004 Volcanic stratigraphy, structural controls, and mineralization in the San Cristobal Ag-Zn-Pb deposit, southern Bolivia *J. South Am. Earth Sci.* **16** 667–83

Ramos Collorana W, Marchionni D, Baldellón Pedraza E, Fernández R and Ramayo Cortéz L 2002 Procesamiento-interpretación de imágenes Landsat TM en la prospección minera del suroeste de Bolivia: control litológico y estructural en la distribución espacial de los depósitos minerales *Proc. SELPER 2002* pp 1–11

Riller U, Petrinovic I, Ramelow J, Strecker M and Oncken O 2001 Late Cenozoic tectonism, collapse caldera and plateau formation in the central Andes *Earth Planet. Sci. Lett.* **188** 299–311

Rowlands A and Sarris A 2007 Detection of exposed and subsurface archaeological remains using multi-sensor remote sensing *J. Archaeological Sci.* **34** 795–803

Salisbury M J, Jicha B R, Shanaka L S, Singer B S, Jiménez N C and Ort M H 2011 $^{40}Ar/^{39}Ar$ chronostratigraphy of Altiplano-Puna volcanic complex ignimbrites reveals the development of a major magmatic province *Geol. Soc. Am. Bull.* **123** 821–40

Schnurr W B W, Trumbull R B, Clavero J, Hahne K, Siebel W and Gardeweg M 2007 Twenty-five million years of silicic volcanism in the southern central volcanic zone of the Andes: Geochemistry and magma genesis of ignimbrites from 25 to 27°S, 67 to 72°W *J. Volcanol. Geotherm. Res.* **166** 17–46

Soler M M, Caffe P J, Coira B L, Onoe A T and Kay S M 2007 Geology of the Vilama caldera: a new interpretation of a large-scale explosive event in the Central Andean plateau during the Upper Miocene *J. Volcanol. Geotherm. Res.* **164** 27–53

Sparks R S, Folkes C B, Humphreys M C S, Barfod D N, Clavero J, Sunagua M C, McNutt S R and Pritchard M E 2008 Uturuncu volcano, Bolivia: volcanic unrest due to mid-crustal magma intrusion *Am. J. Sci.* **308** 727–69

Suarez Soruco R 2000 Bolivian geology compendium *Rev. Tec. Yacimientos Petroliferos Fiscales Bolivianos* **18** 1–215

Van Buren M and Mill B 2005 Huayrachinas and tocochimbos: traditional smelting technology of the southern Andes *Latin Am. Antiquity* **16** 3–25

Watts R B, de Silva S L, Jimenez de Rios G and Croudace I 1999 Effusive eruption of viscous silicic magma triggered and driven by recharge: a case study of the Cerro Chascon-Runtu Jarita Dome Complex in Southwest Bolivia *Bull. Volcanol.* **61** 241–64

Zappettini E O (coord) 2005 Metallogenic map of South America 1:5.000.000 *Anales* vol 44 (Buenos Aires: Instituto de Geología y Recursos Minerales) pp 1–287 (explanatory text)